Energy Conversion and Management 50 (2009) 2613–2621

Contents lists available at ScienceDirect

Energy Conversion and Management

journal homepage: www.elsevier.com/locate/enconman

Experiments during flow boiling of a R22 drop-in: R422D adiabatic pressure gradients

A. Rosato [a,*], A.W. Mauro [a], R. Mastrullo [a], G.P. Vanoli [b]

[a] D.E.TE.C., Facoltà di Ingegneria, Università degli Studi di Napoli Federico II, p.le Tecchio 80, 80125 Napoli, Italy
[b] Dipartimento di Ingegneria, Università degli Studi del Sannio, corso Garibaldi 107, Palazzo dell'Aquila Bosco Lucarelli, 82100 Benevento, Italy

ARTICLE INFO

Article history:
Received 3 November 2008
Accepted 8 June 2009
Available online 9 July 2009

Keywords:
R422D
R22
Drop-in
Pressure drops
Flow boiling
Dry-expansion evaporator

ABSTRACT

R22, the HCFC most widely used in refrigeration and air-conditioning systems in the last years, is phasing-out. R422D, a zero ozone-depleting mixture of R125, R134a and R600a (65.1%/31.5%/3.4% by weight, respectively), has been recently proposed as a drop-in substitute. For energy consumption calculations and temperature control, it is of primary importance to estimate operating conditions after substitution. To determine pressure drop in the evaporator and piping line to the compressor, in this paper the experimental adiabatic pressure gradients during flow boiling of R422D are reported for a circular smooth horizontal tube (3.00 mm inner radius) in a range of operating conditions of interest for dry-expansion evaporators.

The data are used to establish the best predictive method for calculations and its accuracy: the Moreno-Quibèn and Thome method provided the best predictions for the whole database and also for the segregated data in the annular flow regime.

Finally, the experimental data have been compared with the adiabatic pressure gradients of both R22 and its much used alternative R407C available in the literature.

1. Introduction

R22 is still widely used as working fluid in the majority of systems for air-conditioning and refrigeration. The political decisions [1,2] that scheduled its phase-out, due to its high ozone depletion potential (ODP), have been forced through major changes. During last years, new trends in the use of refrigerants established depending on the application field, as highlighted in [3–5].

The substitution of R22 is an operation that interests a lot of plants which are expected still working after its phase-out. The drop-in candidates for R22 have been checked for environmental and safety requirements, compatibility with lubricant oil, filters, sealing; moreover they have thermodynamic properties, like vapor pressure curve, vapor density, heat of vaporization and volumetric refrigerating capacity comparable to R22. Among the candidates, to establish the best substitute in a specified system it is necessary to estimate energy consumptions after the substitution. Consequently, the new balancing point of components has to be determined, requiring pressure drop and heat transfer calculations inside heat exchangers.

R407C, largely used to retrofit R22, have got a special attention from the industry with the expectation of similar energy efficiency without major changes in the system. R407C is a ternary blend of HFC compounds (23% of R32, 25% of R125 and 52% of R134a by weight). It has no chlorine content and a modest GWP (1650). It is non-flammable and non-toxic. Its main thermophysical properties are close to those of R22, but it has the disadvantage of not being suitable with mineral or alkylbenzene oils. However, in comparison with R22, experimental tests carried out with R407C have pointed out a reduction in the energetic performances with a larger environmental impact [6].

Many companies have expended much effort to develop and to identify the refrigerants able to increase the energy efficiency of a refrigerating system, depending on its application. In air-conditioning systems by direct expansion, the refrigerant R422D (commercially known as ISCEON MO29) has been recently proposed as a drop-in refrigerant to R22. R422D, originally designed to replace R22 in existing direct expansion water chiller systems, actually is also used in residential and commercial air-conditioning and low and medium temperature refrigeration systems. In spite of R407C, R422D is compatible with traditional and new lubricants, including mineral oils, alkylbenzene and polyol ester: no change of lubricant type during retrofit of R22 is required. Only minor equipment modifications such as for sealing, filter drier or expansion device adjustments could be required in some applications. R422D is a non-ozone-depleting, non-flammable, non-toxic, ternary mixtures of R125, R134a and R600a (65.1%/31.5%/3.4% by weight, respectively). The small percentage of isobutane promotes adequate oil return in properly piped systems with oil separators.

* Corresponding author. Tel.: +39 081 7682304; fax: +39 081 2390364.
E-mail address: antonio.rosato@unina.it (A. Rosato).

0196-8904/$ - see front matter © 2009 Elsevier Ltd. All rights reserved.
doi:10.1016/j.enconman.2009.06.001

Nomenclature

Latin letters

A	annular flow
C	parameter in Lockhart and Martinelli's equation
COP	coefficient of performance
D	dryout
G	refrigerant mass flux (kg/m^2 s)
GWP	global warming potential
I	intermittent flow
i	specific enthalpy (kJ/kg)
i_{lv}	latent heat of vaporization (kJ/kg)
L	length (m)
M	mist flow
$\dot{m}$	mass flow rate (kg/s)
n	number of points
ODP	ozone-depleting potential
p	pressure (bar)
$\dot{Q}$	power (W)
r	radius (m)
R	electrical resistance (Ω)
sd	standard deviation (%)
t	temperature (K)
V	voltage (V)
$\dot{V}$	volume flow (m^3/s)
w	velocity (m/s)
x	vapor quality
X	Martinelli parameter
z	abscissa along the tube (m).

Greeks

δ	uncertainty
Δ	difference
ε_i	error (%)
$\bar{\varepsilon}$	mean error (%)
$\lvert\bar{\varepsilon}\rvert$	mean absolute error (%)
ϕ	two-phase multiplier
λ	predicted percentage within ± 30% deviation
μ	dynamic viscosity (μPas)
ρ	density (kg/m^3)

Subscripts

A	annular flow
ATS	adiabatic test section
cr	critical
DTS	diabatic test section
exp	experimental
i	inner
I	intermittent flow
in	inlet
in_evap	evaporator inlet
l	liquid
lo	corresponding to the liquid phase flowing alone
M	mist flow
o	outer
PH	preheater
$pred$	predicted
S	slug flow
SW	stratified-wavy flow
sat	saturation for R22, bubble-point for R407C and R422D
tt	turbulent–turbulent flow
v	vapor
vo	corresponding to the vapor phase flowing alone

In comparison to R22, R422D has a higher GWP (2230), it is more expensive and reacts with aluminium.

Recently Dispenza et al. [7] have compared experimentally the performances of R22 and R422D as working fluids in vapor compression refrigerating plants. The results are reported at the same conditions at the evaporator in terms of refrigerating load and secondary fluid temperature. The COP of R422D is lower than R22 by about 25% at higher evaporating temperatures. By a cross comparison of the works in [6,7], we could retain that, for evaporating temperatures of air-conditioning systems, performances of R422D and R407C are comparable.

The results of a bibliographic research showed that there are many experimental studies on flow boiling of refrigerant HFC mixtures [8], while no data on R422D two-phase pressure drops are available. As a consequence, there are no special prediction methods for R422D and it is not sure if the available correlations apply well to this fluid. Besides, it is not available a flow pattern map to predict the two-phase flow transitions developed specifically for R422D.

In this article, the attention is focused on the pressure drop estimation inside evaporators. Preliminarily the properties of R422D that influence two-phase pressure drops will be discussed and compared to those of R22 and R407C. Then the experimental adiabatic pressure gradients of R422D during flow boiling in a smooth, horizontal, circular stainless steel tube with an inner radius of 3.00 mm are reported: 15 tests were carried out obtaining 163 experimental points in operating conditions commonly encountered in dry-expansion evaporators. The refrigerant mass flux varied within the range from 198 to 350 kg/m^2 s, the evaporating pressures within the range from 4.0 to 7.8 bar (bubble-point temperature within the range from −9.2 to 11.8 °C) and the vapor quality within the range from 0.13 to 0.99.

The results of a statistical comparison to predictive methods are reported in order to establish the best one for R422D pressure drop calculations.

Finally, the obtained R422D experimental data are compared with adiabatic pressure gradients available in literature for R22 and R407C in similar operating conditions (tube geometry and inner diameter, evaporating temperature, refrigerant mass flux).

2. Thermodynamic analysis

Table 1 compares the characteristics of R422D that influence two-phase pressure drops with those of R22 and R407C. All values have been obtained by means of REFPROP 7.0 [9].

Table 1
Properties of refrigerants at 0 °C.

Refrigerant	R22	R407C	R422D
Flammability/toxicity	NO/no	NO/no	NO/no
ODP	0.055	0	0
GWP	1700	1650	2230
Molar mass (kg/kmol)	86.5	86.2	109.9
t_{cr} (°C)	96.1	86.0	79.5
p_{cr} (bar)	49.9	46.3	39.0
p_{sat} (bar)	5.0	5.7	5.4
p_{sat}/p_{cr}	0.10	0.12	0.14
ρ_l (kg/m^3)	1281.5	1236.2	1250.3
ρ_v (kg/m^3)	21.2	22.8	30.9
ρ_v/ρ_l	0.017	0.018	0.025
μ_l (μPa s)	216.0	212.1	221.1
μ_v (μPa s)	11.4	12.1	11.8
μ_l/μ_v	19.0	17.6	18.7
i_{lv} (kJ/kg)	205.0	217.3	150.6

The empirical method of Jung and Radermacher [10] considers two-phase pressure drops inversely proportional to the reduced pressure: from table 1 it results that R22 and R407C have a reduced pressure 28% and 11% lower than R422D.

The vapor to liquid density ratio influences the transition among the different flow regimes (at decreasing the vapor to liquid density ratio the vapor quality corresponding to the flow regime transitions "*I–A*", "*A–D*" and "*D–M*" becomes larger [11,12]) and thus the pressure drops. Besides a higher density ratio of vapor to liquid results in a smaller change in velocity for a fixed mass flow rate during evaporation.

Moreover two-phase frictional pressure gradients can be obtained from the single-phase pressure gradients:

$$\left(\frac{dp}{dz}\right)_{\text{two-phase}} = \phi_l \left(\frac{dp}{dz}\right)_{lo} \tag{1}$$

$$\left(\frac{dp}{dz}\right)_{\text{two-phase}} = \phi_v \left(\frac{dp}{dz}\right)_{vo} \tag{2}$$

Lockhart and Martinelli [13] proposed a generalized correlation method to predict the two-phase multipliers ϕ_l and ϕ_v based on adiabatic two-phase flow experiments:

$$\phi_l = \left(1 + \frac{C}{X} + \frac{1}{X^2}\right)^{1/2}$$

$$\phi_v = (1 + CX + X^2)^{1/2}$$

where X is the Martinelli parameter and C is a constant depending of the flow regime associated to the vapor and liquid phase. For circular smooth tubes and turbulent–turbulent flow it results $X = X_{tt} = \left(\frac{\rho_v}{\rho_l}\right)^{0.5}\left(\frac{\mu_l}{\mu_v}\right)^{0.1}\left(\frac{1-x}{x}\right)^{0.9}$ and $C = 20$. At increasing X_{tt}, ϕ_l decreases, while ϕ_v becomes larger. From Table 1 it can be observed that, compared to R422D, R22 and R407C have a lower $\frac{\rho_v}{\rho_l}$ (33% and 25%, respectively). Regarding the dependence of X_{tt} from liquid to vapor viscosity ratio, there are no obvious difference among the fluids. From Eqs. (1) and (2), using Blasius correlation [14] to calculate pressure drop in turbulent single-phase flow and assuming the same refrigerant mass flow rate, it can be obtained:

$$\frac{(\Delta p)_{\text{two-phase,R422D}}}{(\Delta p)_{\text{two-phase,R22(R407C)}}} = \left(\frac{\mu_{\text{R422D}}}{\mu_{\text{R22(R407C)}}}\right)^{\frac{1}{4}}\left(\frac{\rho_{\text{R22(R407C)}}}{\rho_{\text{R422D}}}\right)\left(\frac{\phi_{\text{R422D}}}{\phi_{\text{R22(R407C)}}}\right) \tag{3}$$

From Fig. 1 it results that expected two-phase pressure drops of R422D should be lower than those corresponding to R22 and R407C for all values of vapor quality. The differences become more evident using Eq. (2). The results showed in Fig. 1 are due to the fact that, for all values of vapor quality, $\phi_{1,\text{R422D}}$ is lower than $\phi_{1,\text{R22}}$ and $\phi_{1,\text{R407C}}$, while R22 and R407C show a ϕ_v larger than that pertaining to R422D. However the two-phase pressure drop ratio obtained in Eq. (3) is dependent not only from the two-phase multipliers, but also from the density and the viscosity of the fluids. A higher density results in a smaller velocity for a fixed mass flow rate during evaporation and, compared to R22 and R407C, R422D has about the same liquid density, but a vapor density larger (31% and 26%, respectively). Concerning the viscosity, it is important to consider that a higher viscosity, particularly of the liquid phase, results in larger pressure drop: the liquid and vapor viscosities of R422D are almost equal to those of the other fluids (2–4% of percentage difference).

Eq. (3) has been obtained hypothesizing the same refrigerant mass flow rate. However in a refrigeration system, the mass flow rate is connected to the desired cooling capacity through the heat of vaporization, so that the fluid velocity in a circular tube at a given cooling capacity can be expressed as:

$$w = \frac{\dot{V}}{\pi r^2} = \frac{\dot{m}}{\rho \pi r^2} = \frac{\dot{Q}}{\rho \pi r^2 (i_v - i_{in\_evap})} = \frac{\dot{Q}}{\rho \pi r^2 i_{fg}(1 - x_{in\_evap})}$$

Combining Blasius correlation [14] and Eqs. (1) and (2), and assuming the same refrigerating power, one can obtain:

$$\frac{(\Delta p)_{\text{two-phase,R422D}}}{(\Delta p)_{\text{two-phase,R22(R407C)}}} = \left(\frac{\mu_{\text{R422D}}}{\mu_{\text{R22(R407C)}}}\right)^{\frac{1}{4}}\left(\frac{\rho_{\text{R22(R407C)}}}{\rho_{\text{R422D}}}\right)\left(\frac{\phi_{\text{R422D}}}{\phi_{\text{R22(R407C)}}}\right) \times \left(\frac{i_{lv,\text{R22(R407C)}}}{i_{lv,\text{R422D}}}\right)^{\frac{7}{4}}\left(\frac{1 - x_{in\_evap,\text{R22(R407C)}}}{1 - x_{in\_evap,\text{R422D}}}\right)^{\frac{7}{4}}$$

where x_{in_evap} is calculated under the following conditions: evaporation temperature of 0 °C, condensing temperature of 40 °C, no superheat at the compressor inlet and no subcooling at the condenser outlet, no heat losses to the ambient and no pressure drop in the pipelines and heat exchangers. From Fig. 2 it is evident that expected two-phase pressure drops of R422D should be larger than those corresponding to R22 and R407C for all values of vapor quality. The differences are due to the fact that, compared to R422D, R22

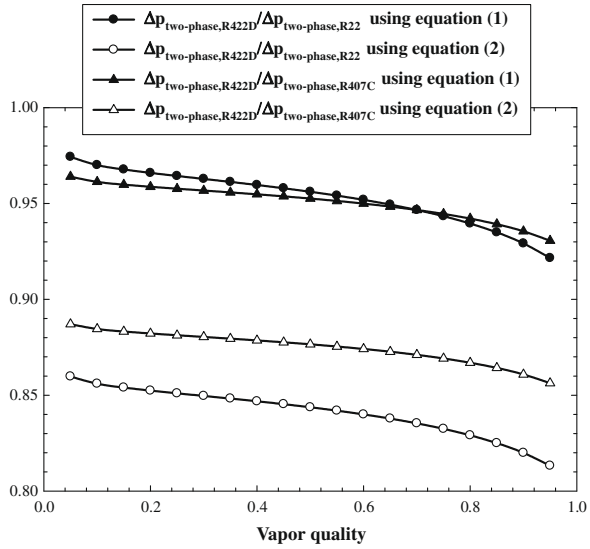

Fig. 1. Comparison of R422D two-phase pressure drops with those of R22 and R407C at the same refrigerant mass flux using the Lockart–Martinelli correlation [13].

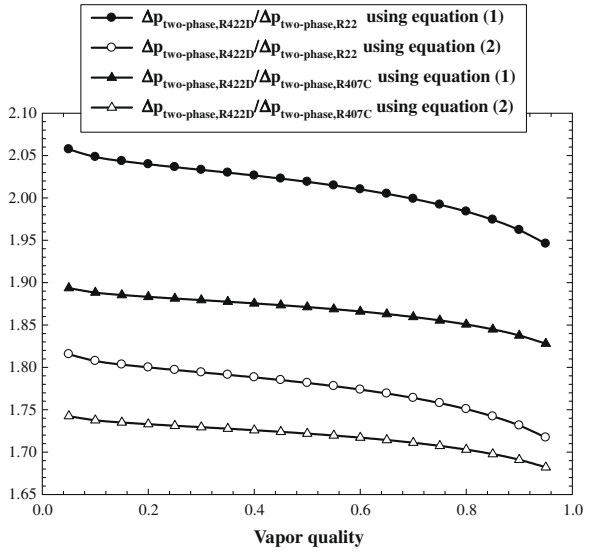

Fig. 2. Comparison of R422D two-phase pressure drops with those of R22 and R407C at the same refrigerating power using the Lockart–Martinelli correlation [13].

and R407C have much higher latent heat of evaporation (36% and 44%, respectively) and much lower vapor quality at the evaporator inlet (38% and 22%, respectively). On the other hand, we have to consider that R422D has a slope of the vapor pressure curve slightly higher than that of R22: this gives a smaller temperature change for a given pressure drop in the evaporator.

3. Experimental plant

A schematic view of the plant is shown in Fig. 3. The experimental apparatus allows to measure the local pressure gradient during flow boiling. The refrigerant loop consists of a magnetic gear pump, a preheater, an adiabatic and a diabatic test section, a shell-and-tube heat exchanger, a brazed plate heat exchanger and a tube-in-tube subcooler.

The magnetic gear pump drives the fluid coming from the liquid reservoir. The refrigerant mass flux can be modified varying the electric motor speed by an inverter. The refrigerant, in sub-cooled conditions, passes first through the preheater where heat is supplied to the fluid by fibreglass heating tapes (four fibreglass heating tapes with a nominal power of 830 W at 240 V (AC) for each one); changing the voltage it is possible to modify the thermal power and to obtain the desired quality at the adiabatic test sections inlet. After the preheater, the fluid flows through the diabatic test section and then enters the adiabatic test section: it is a 1000.0 mm ($\delta(L_{ATS})$=0.5 mm), circular, smooth, horizontal, stainless steel (type AISI 304) tube with an inner radius of 3.00 mm ($\delta(r_{i,ATS})$ = 0.05 mm) and an outer radius of 4.00 mm ($\delta(r_{o,ATS})$=0.05 mm). The refrigerant then exits this test section and condenses in a shell-and-tube heat exchanger and in a brazed plate heat exchanger. Before returning to the pump, the refrigerant is sub-cooled in a tube-in-tube heat exchanger. The coolant is an auxiliary fluid (TEMPER) contained in a storage tank of 200 dm^3. It can be chilled down to −30 °C by a R404A auxiliary refrigerating plant and it is circulated by a magnetic gear pump connected to an inverter. By adjusting the refrigerant charge, the TEMPER inlet temperature and mass flow rate, it is possible to modify and hold constant the refrigerant evaporating pressure in the test section. To avoid heat gains, heavy insulation was provided for all parts of the plant.

4. Data acquisition, data reduction and uncertainty analysis

Table 2 summarizes the measurement characteristics of the plant instrumentation. For data acquisition and storage, a personal computer connected with a 16 bit resolution data acquisition system, provided with a software for monitoring experimental values, is used. The logging of signals from all the sensors is performed on all the channels for 100 s with 1.0 Hz acquisition frequency and the average values of each channel are stored. If the deviation of each value from its average value is lower than a fixed quantity, steady-state conditions are assumed.

The total pressure drop Δp_{ATS} over the adiabatic test section is measured by one of two different piezoelectric differential pressure transducers (operating ranges: 0–10 kPa and 0–100 kPa, uncertainty: 0.075% of full scale) depending on the test conditions. The frictional pressure drop is assumed to be equal to the total pressure drop, since there is no change in static head and it was verified that the change of momentum between phases can be neglected in the operating conditions of this study.

The vapor quality at the inlet of the adiabatic test section is obtained evaluating the specific enthalpy $i_{in,ATS}$ and the absolute pressure $p_{in,ATS}$.

$i_{in,ATS}$ is calculated from an energy balance between the inlet of the preheater and the inlet of the adiabatic test section, assuming negligible the heat gain in the piping between the preheater and the diabatic test section and between the two test sections:

$$i_{in,ATS} = i_{in,PH} + \frac{\dot{Q}_{PH}}{\dot{m}} + \frac{\dot{Q}_{DTS}}{\dot{m}}$$

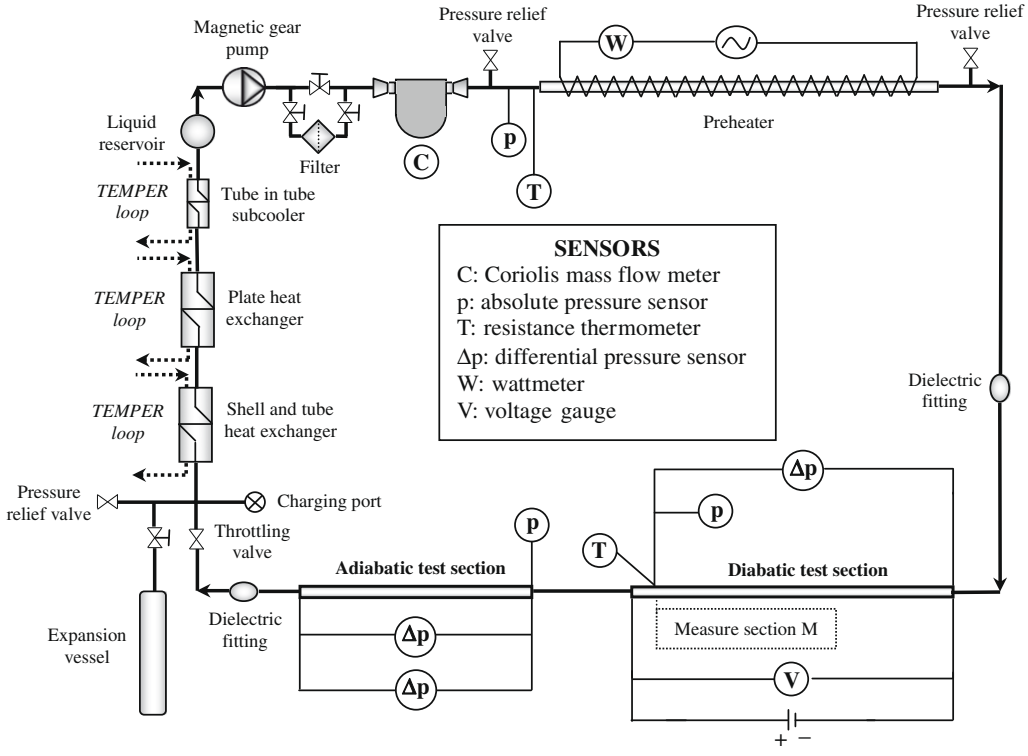

Fig. 3. Experimental apparatus scheme.

Table 2
Measurement equipment.

Measurement	Device	Calibration range	Uncertainty
Δp_{ATS}	Piezoelectric differential pressure transducer	0–10 kPa	±0.075% of full scale
	Piezoelectric differential pressure transducer	0–100 kPa	±0.075% of full scale
$p_{in,ATS}$	Piezoelectric absolute pressure transducer	0–50 bar	±0.1% of full scale
$t_{in,PH}$	Probe resistance thermometer Pt100	−50–100 °C	±0.15 °C
$p_{in,PH}$	Piezoelectric absolute pressure transducer	0–50 bar	±0.1% of range
Q_{PH}	Wattmeter	0–3600 W	±0.2% of reading + 0.02% of full scale
V_{DTS}	Electronic voltage transducer	0–10 V	±0.19% of reading + 0.01% of full scale
m	Coriolis mass flow meter	0–1.8 kg s^{-1}	±0.05% of reading
p_{sat}	Piezoelectric absolute pressure transducer	0–50 bar	±0.1% of full scale

The specific enthalpy at the inlet of the preheater is evaluated from the absolute pressure $p_{in,PH}$ and temperature $t_{in,PH}$. The heating power $\dot{Q}_{PH}$ provided to the refrigerant in the preheater is measured with a wattmeter, while the heating power $\dot{Q}_{DTS}$ supplied to the fluid in the diabatic test section is determined as $\frac{V_{DTS}^2}{R_{DTS}}$, where R_{DTS} is the electrical resistance of the heated channel (0.030209 Ω ± 0.045 mΩ at −4.90 °C and 0.039159 ± 0.056 mΩ at 35.00 °C) and V_{DTS} is the voltage measured at the diabatic test section. The refrigerant mass flow rate $\dot{m}$ is measured by a Coriolis effect mass flow meter working in the liquid line.

The absolute pressure $p_{in,ATS}$ is directly measured by means of a piezoelectric absolute pressure transducer.

All the thermodynamic properties are calculated by the software REFPROP [10].

The uncertainties for the pressure gradient and for the vapor quality at the inlet of the adiabatic test section were calculated according to the single-sample uncertainty analysis suggested by Moffat [15].

5. Preliminary tests

The reliability of the measurements was verified through three different checks: (i) single-phase R134a pressure drop measurements, (ii) single-phase energy balance and (iii) repeatability of the measurements.

Twenty experiments were carried out with mass velocities ranging from 701 to 1005 kg/m^2 s covering a range of Reynolds numbers from 13,251 up to 22,066 (turbulent flow).

The R134a liquid phase pressure drops have been measured and compared with those obtained with the Blasius correlation [14] which is valid for smooth tubes and turbulent flow. The comparison has been characterized by the following parameters:

$$\varepsilon_i = \left(\frac{\Delta p_{pred,i} - \Delta p_{exp,i}}{\Delta p_{exp,i}}\right)$$

$$\bar{\varepsilon} = \frac{1}{n}\sum_{i=1}^{n}\varepsilon_i$$

$$|\bar{\varepsilon}| = \frac{1}{n}\sum_{i=1}^{n}|\varepsilon_i|$$

$$\mathrm{sd} = \sqrt{\frac{1}{n}\sum_{i=1}^{n}(\varepsilon_i - \bar{\varepsilon})^2}$$

From Fig. 4, it can be seen that Blasius correlation [14] predicts the experimental data with a mean error of 0.8%, an absolute mean error of 3.4% and a standard deviation equal to 7.3%.

The energy balance absolute mean error was always less than 3.5%, which is a good result for this type of experiments.

The measurement repeatability was investigated in a fixed operating condition ($G \approx 300$ kg/m^2 s, $p_{sat} \approx 3.5$ bar) four times: Fig. 5 shows a good agreement of the adiabatic pressure gradient data. The performed preliminary tests showed an instrumentation calibration and overall system performance consistent with the desired accuracy.

6. Experimental results

In this work R422D adiabatic pressure gradient were experimentally evaluated. We carried out 15 tests obtaining 163 points. The experiments were performed varying the refrigerant mass fluxes within the range from 198 to 350 kg/m^2 s, the evaporating pressures within the range from 4.0 to 7.8 bar (bubble-point temperature within the range from −9.2 to 11.8 °C) and the vapor quality within the range from 0.13 to 0.99.

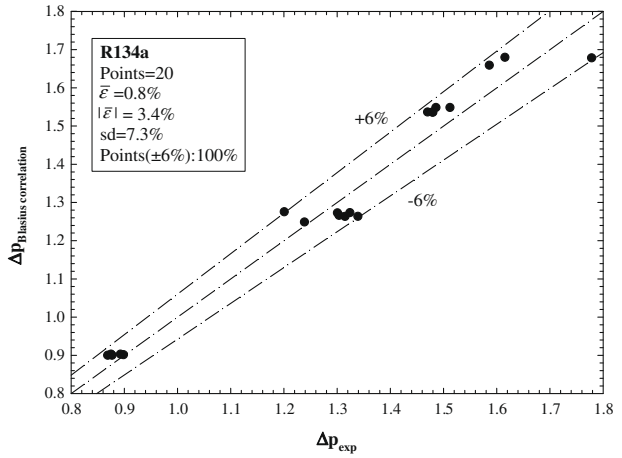

Fig. 4. Comparison of single-phase pressure drop measurements to predictions by Blasius [14] correlation.

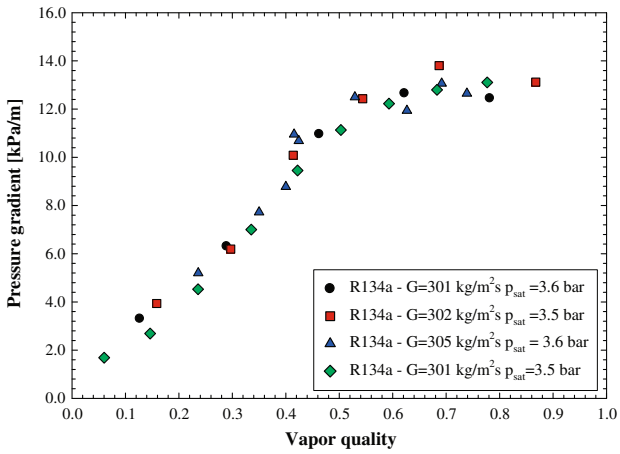

Fig. 5. Pressure gradients of R134a as a function of vapor quality: a fixed operating condition ($G \approx 300$ kg/m^2 s and $p_{sat} \approx 3.5$ bar) investigated four times.

Table 3
The operating conditions.

G (kg/m^2 s)	p_{sat} (bar)	t_{sat} (°C)	Δx_S	Δx_I	Δx_A	Δx_{SW}	Δx_M	Δx_{exp}
198	6.3	4.7	0.01–0.25	0.25–0.40	0.40–0.89	0.89–0.97	0.97–0.98	0.27–0.99
200	4.1	−8.5	0.01–0.22	0.22–0.35	0.35–0.90	0.90–0.97	0.97–0.98	0.26–0.91
205	4.8	−3.8	0.01–0.22	0.22–0.37	0.37–0.90	0.90–0.97	0.97–0.98	0.36–0.99
249	6.3	4.7	0.01–0.15	0.15–0.40	0.40–0.92	0.92–0.97	0.97–0.98	0.2–0.98
250	4.8	−3.8	0.01–0.15	0.15–0.37	0.37–0.93	0.93–0.97	0.97–0.98	0.31–0.98
252	4.1	−8.5	0.01–0.14	0.14–0.35	0.35–0.93	0.93–0.97	0.97–0.98	0.35–0.99
294	4.1	−8.5	0.01–0.10	0.10–0.35	0.35–0.94	0.94–0.97	0.97–0.98	0.17–0.98
300	4.0	−9.2	0.01–0.10	0.10–0.34	0.34–0.95	0.95–0.97	0.97–0.98	0.17–0.90
300	4.8	−3.8	0.01–0.10	0.10–0.34	0.34–0.95	0.95–0.97	0.97–0.98	0.17–0.92
301	6.3	4.7	0.01–0.10	0.10–0.40	0.40–0.94	0.94–0.97	0.97–0.98	0.18–0.93
301	7.8	11.8	0.01–0.10	0.10–0.43	0.43–0.94	0.94–0.97	0.97–0.98	0.14–0.99
346	4.0	−9.2	0.01–0.08	0.08–0.34	0.34–0.96	0.96–0.97	0.97–0.98	0.19–0.65
349	4.8	−3.8	0.01–0.08	0.08–0.37	0.37–0.95	0.95–0.97	0.97–0.98	0.15–0.88
350	6.3	4.7	0.01–0.07	0.07–0.40	0.40–0.95	0.95–0.97	0.97–0.98	0.13–0.89
350	7.8	11.8	0.01–0.06	0.06–0.43	0.43–0.95	0.95–0.97	0.97–0.98	0.15–0.94

The operating conditions investigated are summarized in Table 3: in this table, the refrigerant mass flux, the evaporating pressure (and the corresponding bubble-point temperature) and the vapor quality range are specified for each test. The relative measurement uncertainty in the evaluation of the pressure gradients ranges between 1.4% and 4.6%, while the uncertainty in the evaluation of the vapor quality at the inlet of the test section is always lower than 3.3%.

Since the pressure gradients are influenced by the liquid and vapor phase distributions, the flow patterns have been identified by a flow pattern map [16,17], even if it has not been developed specifically for R422D. In Table 3 the range of vapor qualities corresponding to the different flow regimes are also reported for each operating condition. The results showed that, for the considered operating conditions, the flow pattern map does not allow the stratified flow, the stratified and slug flow and the dryout; a limited number of cases returns mist (seven points) or stratified-wavy (five points) flow regime. None experimental point is in the slug flow regime. Intermittent flow regime is the flow regime for 43 points. In the most of cases (108 points) the flow regime is annular (67% of the experimental database).

Fig. 6 depicts the pressure gradient of R422D as a function of vapor quality at varying refrigerant mass flux from 198 to 350 kg/m^2 s for: (a) $t_{sat} = -8.5$ °C, (b) $t_{sat} = -3.8$ °C, (c) $t_{sat} = 4.7$ °C and (d) $t_{sat} = 11.8$ °C.

As expected, the bubble-point temperature strongly influences the pressure gradients for a fixed refrigerant mass flux: increasing the bubble-point temperature the pressure gradients decrease (mainly for values of vapor quality lower than about 85%). Indeed, as the evaporating pressure increases, the liquid viscosity decreases and the liquid density becomes higher (the increase of the liquid density leads to the rise of vapor–liquid mixture and, therefore, to the decrease of the refrigerant velocity). From $t_{sat} = -8.5$ °C to $t_{sat} = 4.7$ °C the R422D liquid viscosity and density become about 20% lower and 50% higher, respectively. Similar considerations can be repeated for the trends observed at $t_{sat} \approx -9$ °C, that have not been reported in this figure. Besides, the plots clearly show that the increase of the mass flow rate, for fixed thermodynamic properties, increases the pressure gradients because the mean velocity of the vapor–liquid mixture becomes higher.

Concerning the influence of vapor quality, it can be noticed the characteristic rise in two-phase frictional pressure gradient with rising vapor quality, a peak at high vapor quality, and the subsequent falloff as the vapor quality approaches 100%. In fact for low vapor qualities the flow regime is, in most cases, intermittent in the tested operating conditions. In this flow regime the pressure drops are mainly influenced from the friction of the liquid along the tube wall. When the quality increases, the flow regime tends to become annular and slope of the pressure gradient curve increases. For higher vapor quality, between about 65% and 90%, the liquid thickness dries, the friction reduces and, as a consequence, pressure gradient decreases. It is interesting to notice that in each operating condition there is not an increasing trend with vapor quality after the falloff, so the transition to mist flow probably never occurred.

7. Comparison with predictive methods

Many predictive methods have been developed over the past decades: however, there are no such prediction methods based on R422D experimental data. To determine the best predictive method for the tested operating conditions, the R422D experimental data were compared to the phenomenological method of Moreno-Quibèn and Thome [18] and to the empirical methods of Friedel [19], Grönnerud [20], Müller-Steinaghen and Heck [21] and Jung and Radermacher [22].

The results for the whole database and for the segregated data by flow regimes (annular and intermittent) are reported in Table 4. To segregate the data by flow regime the flow pattern map by Wojtan et al. [16,17] was used.

For the entire database, it can be observed that all correlations, except Müller-Steinaghen and Heck method, tend to overpredict the experimental data. Even if Friedel method gave the best mean error (2.7%), Moreno-Quibèn and Thome correlation provided the lowest absolute mean error (32%) and is able to predict the 77.3% of data within ± 30%; Jung and Radermacher correlation produces the worst predictions with an absolute mean error of 70.5%. For all methods the standard deviation is high: that one corresponding to Moreno-Quibèn and Thome method is 85.2% and not very different from those of Grönnerud (75.4%) and Müller-Steinaghen and Heck (78.1%) methods. However the above considerations were affected by the data distribution with respect to the flow regimes. The analysis for each flow regime showed different results. In the intermittent region, the method by Müller-Steinaghen and Heck granted the more reliable predictions. Results by Moreno-Quibèn and Thome method were the best in the annular flow regime both for mean error (9.3%) and absolute mean error (16.1%); however its standard deviation (20.0%) is slightly higher than that one corresponding to Friedel and Müller-Steinaghen and Heck correlations (14.0%).

To evaluate how well the predictive methods captured the trends of the pressure drop function, a direct comparison of the methods and the experimental data was carried out: from the anal-

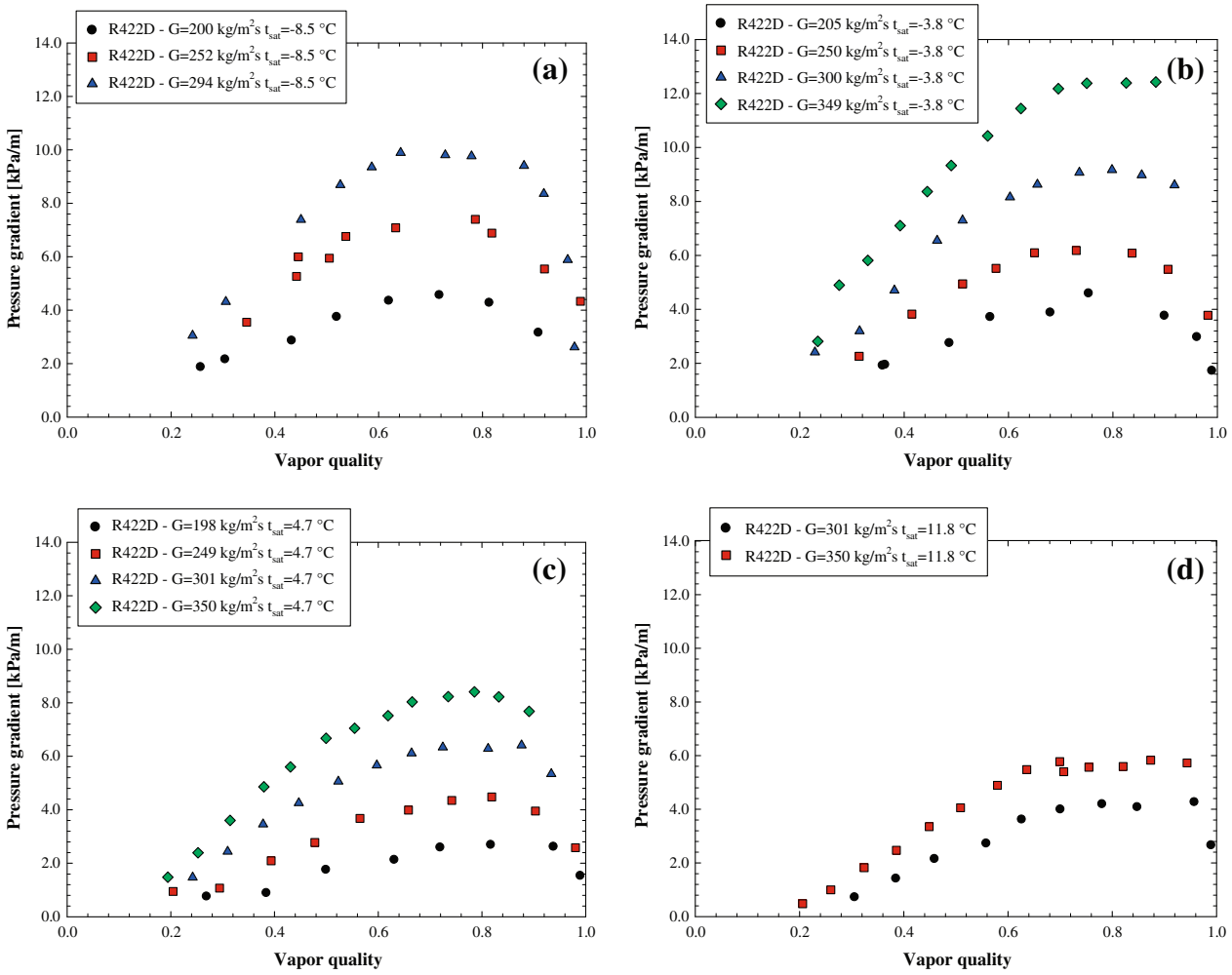

Fig. 6. Pressure gradient of R422D as a function of vapor quality at refrigerant mass flux of about 200 kg/m^2 s, 250 kg/m^2 s, 300 kg/m^2 s and 350 kg/m^2 s for: (a) t_{sat} = −8.5 °C, (b) t_{sat} = −3.8 °C, (c) t_{sat} = 4.7 °C and (d) t_{sat} = 11.8 °C.

Table 4
Results of statistical comparison between the predicted and the experimental pressure drops.

Number of points	Predictive method	$\bar{\varepsilon}$ (%)	$\lvert\bar{\varepsilon}\rvert$ (%)	sd (%)	λ (%)
Whole database					
163	Moreno and Thome [18]	22.7	32.0	85.2	77.3
	Friedel [19]	2.7	41.9	116.4	58.9
	Grönnerud [20]	36.8	43.5	75.4	49.1
	Müller-Steinaghen and Heck [21]	−7.5	37.7	78.1	49.7
	Jung-Radermacher [22]	69.9	70.5	115.7	35.6
Intermittent flow regime					
43	Moreno and Thome [18]	57.3	75.4	159.9	–
	Friedel [19]	75.8	86.7	212.6	–
	Grönnerud [20]	47.6	64.9	138.1	–
	Müller-Steinaghen and Heck [21]	27.9	60.9	140.2	–
	Jung-Radermacher [22]	122.4	124.6	211.0	–
Annular flow regime					
108	Moreno and Thome [18]	9.3	16.1	20.0	–
	Friedel [19]	−25.6	27.1	14.0	–
	Grönnerud [20]	29.4	32.7	28.8	–
	Müller-Steinaghen and Heck [21]	−27.2	27.7	14.3	–
	Jung-Radermacher [22]	46.0	46.0	32.4	–

ysis it was observed that in most cases the Moreno-Quibèn and Thome method best captures the trends in all the range of vapor qualities, even if in some cases it tends to overpredicts the value of vapor quality corresponding to the maximum pressure drop.

8. Comparison of R22 and R407C to R422D pressure drops

In the following we compared our R422D data with the experimental pressure gradients of R22 and R407C available in literature

obtained in the same set of operating conditions (evaporating temperature, refrigerant mass flow rate) from adiabatic experiments. We analyzed only works with horizontal, smooth, circular test tube.

Fig. 7 shows the comparison of pressure gradients measured in this study with those obtained by Wang et al. [23] for R22 at similar evaporating temperature and refrigerant mass flux with a test tube inner diameter of 7.92 mm. Taking into account the differences in the tube inner diameter and bubble-point temperature, we can conclude that, for the operating conditions tested, the R22 pressure gradients are slightly higher than those of R422D.

In Fig. 8 the comparison of pressure gradients obtained in this study with those measured by Wang and Chiang [23] for R407C for two different operating conditions is reported. It can be easily observed that R422D pressure gradients are slightly higher than those corresponding to R407C, mainly for medium–high vapor qualities: it may be caused by the different tube inner diameter, even though the evaporating temperature corresponding to the Wang et al. experiments is quite lower than that pertaining to our tests.

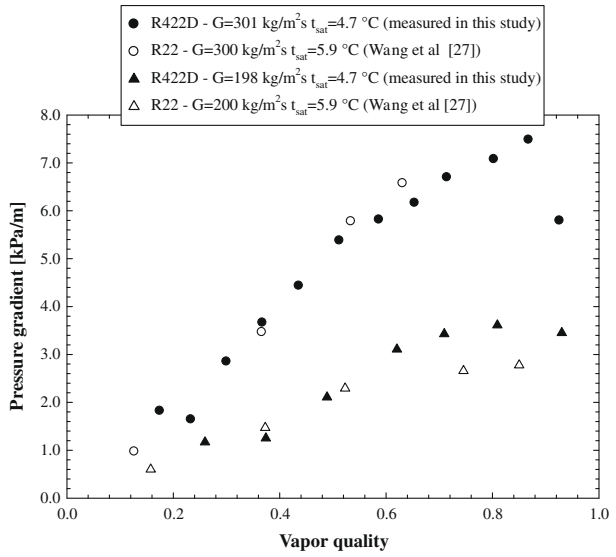

Fig. 7. Comparison of pressure gradients measured in this study with those obtained by Wang et al. [23] for R22 at $G = 200$ and 300 kg/m^2 s, $t_{sat} = 5.9$ °C and $d_i = 7.92$ mm.

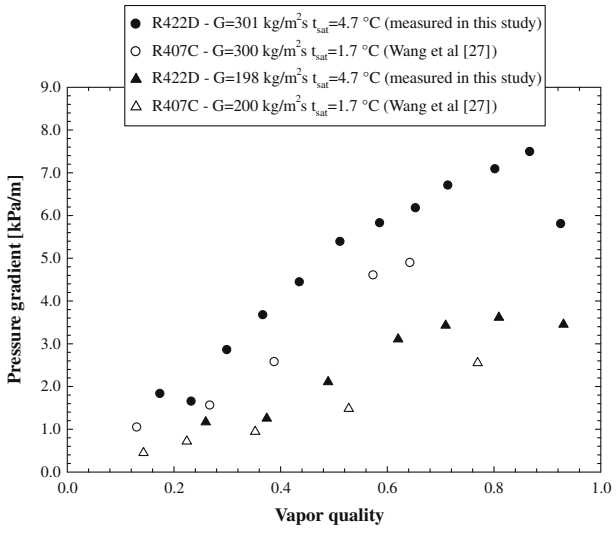

Fig. 8. Comparison of pressure gradients measured in this study with those obtained by Wang et al. [23] for R407C at $G = 200$ and 300 kg/m^2 s, $t_{sat} = 1.7$ °C, $d_i = 7.92$ mm.

9. Conclusions

The scheduled phase-out of HCFCs, particularly R22, has prompted industry to identify new possible alternative. R422D has been recently proposed as a drop-in refrigerant to R22: it is a zero ozone-depleting, non-flammable, non-toxic, zeotropic ternary mixture of R125, R134a and R600a (65.1%/31.5%/3.4% by weight, respectively) that can be used to retrofit R22 without change of lubricant type.

In this paper the experimental adiabatic pressure gradients during flow boiling of R422D were reported. Preliminary tests have ensured appropriate instrumentation calibration and overall system performance of the apparatus. The experiments on R422D were carried out in a range of operating conditions of interest for the dry-expansion evaporator for air-conditioning systems showing the dependence of mass flow rate (from 198 to 350 kg/m^2 s) and evaporating temperature (from −9.2 to 11.8 °C) in a 3.00 inner radius circular smooth horizontal stainless steel tube.

The results were compared against pressure drop predictive methods and the Moreno-Quibèn and Thome method provided the best results.

References

[1] Montreal protocol; 16 September 1987.
[2] EC Regulation 2037/2000.
[3] Cavallini A. Working fluids for mechanical refrigeration. Int J Refrig 1996;19:485–96.
[4] Billiard F. New trends in refrigerating equipment and refrigerants. In: Proceedings of Xth European conference on technological innovations in air conditioning and refrigeration industry, Milan; 2003.
[5] UNEP. Report of the refrigeration, air-conditioning and heat pumps technical options committee; 2006.
[6] Aprea C, Mastrullo R, Renno C, Vanoli GP. An evaluation of R22 substitutes performances regulating continuously the compressor refrigeration capacity. Appli Therm Eng 2004;24:127–39.
[7] Dispenza A, Dispenza C, La Rocca V, Morale M, Panno D, Panno G. Esperimenti sulle prestazioni di fluidi sostitutivi dell'R22 negli impianti frigoriferi. In: 63° Congresso Nazionale ATI, Palermo; 23–26 September 2008.
[8] Greco A. Convective boiling of pure and mixed refrigerants: an experimental study of the major parameters affecting heat transfer. Int J Heat Mass Transfer 2008;51:896–909.
[9] Lemmon EW, Mc Linden MO, Huber ML. NIST standard reference database 23, Version 7.0. Physical and chemical properties.
[10] Jung DS, Radermacher R. Prediction of pressure drop during horizontal annular flow boiling of pure and mixed refrigerants. Int J Heat Mass Transfer 1989;12:2435–46.
[11] Kattan N, Thome JR, Favrat D. Flow boiling in horizontal tubes. Part 1: Development of a diabatic two-phase flow pattern map. J Heat Transfer 1998;120:140–7.
[12] Mori H, Yoshida S, Ohishi K, Kokimoto Y. Dryout quality and post dryout heat transfer coefficient in horizontal evaporator tubes. In: Proceedings of 3rd European thermal sciences conference; 2000. p. 839–44.
[13] Lockhart RW, Martinelli RC. Proposed correlation of data for isothermal two-phase, two-component in pipes. Chem Eng Process 1949;45:39–48.
[14] McAdams WH. Heat transmission. Mc Graw-Hill; 1954.
[15] Moffat RJ. Describing uncertainties in experimental results. Exp Therm Fluid Sci 1988;1:3–17.
[16] Wojtan L, Ursenbacher T, Thome JR. Investigation of flow boiling in horizontal tubes: Part I – A new diabatic two-phase flow pattern map. Int J Heat Mass Transfer 2005;48:2955–69.
[17] Wojtan L, Ursenbacher T, Thome JR. Investigation of flow boiling in horizontal tubes: Part II – Development of a new heat transfer model for stratified-wavy, dry-out and mist flow regimes. Int J Heat Mass Transfer 2005;48:2970–85.
[18] Moreno-Quibén J, Thome JR. Flow pattern based two-phase frictional pressure drop model for horizontal tubes, Part II: New phenomenological model. Int J Heat Fluid Flow 2007;28:1060–72.
[19] Friedel L. Improved friction pressure drop correlations for horizontal and vertical two-phase pipe flow. In: European two-phase flow group meeting, Paper E2, Ispra, Italy; 1979.

[20] Grönnerud R. Investigation of liquid hold-up, flow-resistance and heat transfer in circulation type evaporators, Part IV: Two-phase flow resistance in boiling refrigerants. Bull. de l'Inst. du Froid; 1979, Annexe 1972-1.
[21] Müller-Steinhagen H, Heck K. A simple friction pressure drop correlation for two-phase flow in pipes. Chem Eng Process 1986;20:297–308.
[22] Jung DS, Radermacher R. Prediction of pressure drop during horizontal annular flow boiling of pure and mixed refrigerants. Int J Heat Mass Transfer 1989;32:2435–46.
[23] Wang CC, Kuo CS, Chang YJ, Lu DC. Two phase heat transfer and friction characteristics of R-22 and R-407C. ASHRAE Trans 1996;102:830–8.